Available online at www.sciencedirect.com
ScienceDirect
Journal of Power Sources 171 (2007) 79–85
JOURNAL OF POWER SOURCES
www.elsevier.com/locate/jpowsour

Electrochemical performance of $Ba_{0.5}Sr_{0.5}Co_xFe_{1-x}O_{3-\delta}$ ($x = 0.2$–0.8) cathode on a ScSZ electrolyte for intermediate temperature SOFCs

Yong Ho Lim, Jun Lee, Jong Seol Yoon, Chul Eui Kim, Hae Jin Hwang *

School of Materials Science and Engineering, Inha University, Incheon 402-751, Republic of Korea

Received 12 September 2006; received in revised form 16 May 2007; accepted 16 May 2007
Available online 21 May 2007

Abstract

Intermediate temperature solid oxide fuel cell cathode materials (Ba, Sr)$Co_xFe_{1-x}O_{3-\delta}$ [$x = 0.2$–0.8] (BSCF), were synthesized by a glycine-nitrate process (GNP) using $Ba(NO_3)_2$, $Sr(NO_3)_2$, $Co(NO_3)_2{\cdot}6H_2O$, and $Fe(NO_3)_3{\cdot}9H_2O$ as starting materials and glycine as an oxidizer and fuel. Electrolyte-supported symmetric BSCF/GDC/ScSZ/GDC/BSCF cells consisting of porous BSCF electrodes, a GDC buffer layer, and a ScSZ electrolyte were fabricated by a screen printing technique, and the electrochemical performance of the BSCF cathode was investigated at intermediate temperatures (500–700 °C) using AC impedance spectroscopy. Crystallization behavior was found to depend on the pH value of the precursor solution. A highly acidic precursor solution increased the single phase perovskite formation temperature. In the case of using a precursor solution with pH 2, a single perovskite phase was obtained at 1000 °C. The thermal expansion coefficient of BSCF was gradually increased from $24 \times 10^{-6}\,K^{-1}$ for BSCF ($x = 0.2$) to $31 \times 10^{-6}\,K^{-1}$ (400–1000 °C) for BSCF ($x = 0.8$), which resulted in peeling-off of the cathode from the GDC/ScSZ electrolyte. Only the BSCF ($x = 0.2$) cathode showed good adhesion to the GDC/ScSZ electrolyte and low polarization resistance. The area specific resistance (ASR) of the BSCF ($x = 0.2$) cathode was $0.183\,\Omega\,cm^2$ at 600 °C. The ASR of other BSCF ($x = 0.4$, 0.6, and 0.8) cathodes, however, was much higher than that of BSCF ($x = 0.2$).

Keywords: SOFC; BSCF; Cathode; ScSZ; Polarization resistance

1. Introduction

The cathode for solid oxide fuel cells (SOFCs) should possess many properties including high electrical conductivity, high catalytic activity for oxygen reduction, and compatibility with other cell components. Among the necessary properties, the cathode's catalytic activity for oxygen reduction and its compatibility with the electrolyte are of particular importance. From the viewpoint of catalytic activity, many perovskite compounds have been considered and investigated [1–4]. Strontium doped lanthanum manganite (La, Sr)MnO_3 (LSM) is a typical cathode material, but it is limited in use with respect to intermediate temperature SOFCs (IT-SOFCs, operating temperature: 600–800 °C) because of its low oxygen ion conductivity ($10^{-7}\,S\,cm^{-1}$ at 900 °C) [5,6]. On the other hand, doped lanthanum ferrites (La,Sr)(Co,Fe)O_3 (LSCF) have very high oxygen ion conductivity (~$0.2\,S\,cm^{-1}$ at 900 °C), and have been widely investigated as IT-SOFCs cathode material [7–10]. Along with LSCF, doped barium ferrites (Ba,Sr)(Co,Fe)O_3 (BSCF) have drawn interest for application to intermediate temperature (IT)-SOFCs [11–14].

BSCF is a mixed ionic and electronic conductor with high catalytic activity over oxygen reduction and good oxygen ion permeability, and shows excellent performance as a cathode on samarium doped ceria (SDC) electrolyte in an intermediate temperature range [11]. However, most Co-containing cathode materials including BSCF are not compatible with zirconia-based electrolytes with respect to producing an interfacial-insulating layer, thus reducing the catalytic activity of the electrodes [15,16]. Accordingly, the BSCF cathode cannot be applied directly on ZrO_2 electrolyte. A material that is known to be chemically compatible with the BSCF cathode is CeO_2. It possess a higher ionic conductivity than ZrO_2 but cannot be used an electrolyte because of its low mechanical strength and reduction in the fuel atmosphere. Therefore, in order to use BSCF as an IT-SOFCs cathode, it has been proposed that a buffer layer of

* Corresponding author. Tel.: +82 32 860 7521; fax: +82 32 862 4482.
E-mail address: hjhwang@inha.ac.kr (H.J. Hwang).

0378-7753/$ – see front matter © 2007 Elsevier B.V. All rights reserved.
doi:10.1016/j.jpowsour.2007.05.050

gadolinium doped ceria (GDC) be utilized as a protective layer on the ZrO_2 electrolyte [15–18].

In this study, $Ba_{0.5}Sr_{0.5}Co_xFe_{1-x}O_{3-\delta}$ ($x = 0.2$, 0.4, 0.6, and 0.8) (BSCF) powders were synthesized by a combined glycine nitrate process [19–21]. Phase evolution behavior and thermal expansion coefficient variation of the BSCF were investigated in terms of the x value in $Ba_{0.5}Sr_{0.5}Co_xFe_{1-x}O_{3-\delta}$. A BSCF/GDC(buffer layer)/ScSZ/GDC(buffer layer)/BSCF symmetrical cell was fabricated and the effect of the x value on the cathode performance is reported. Catalytic activity of the BSCF cathode was evaluated from impedance spectra analyses at a very low current density.

2. Experimental procedure

2.1. BSCF powder synthesis

$Ba_{0.5}Sr_{0.5}Co_xFe_{1-x}O_{3-\delta}$ ($x = 0.2$, 0.4, 0.6, and 0.8) powders were prepared by a glycine nitrate process (GNP). The procedure is outlined in the flowchart shown in Fig. 1. $Ba(NO_3)_2$ (Acros, 99%), $Sr(NO_3)_2$ (Acros, 99%), $Co(NO_3)_2{\cdot}6H_2O$ (Acros, 99%), and $Fe(NO_3)_3{\cdot}9H_2O$ (Kanto Chemical Co. Inc. 99%) were used as starting raw materials. Glycine (Kanto Chemical Co. Inc. 99%) was used as an oxidizer and fuel. Metal nitrates were dissolved in distilled water and the pH values were adjusted to 0, 1, 2, and 3 by adding ammonia to the solutions. Glycine was then added into the nitrate aqueous solution while stirring (molar ratio of glycine to nitrate is unit). The mixed solution was heated to 320 °C on a hot plate, and the viscosity of the solution increased gradually with time. The viscous gel causes a combustion reaction, and a dark gray BSCF ash remains. The obtained ash was calcined at 1000 °C for 5 h under air to remove any carbon residues remaining in the ash and to form a crystalline structure. The calcined powder was milled for 1 h using a planetary mill to break up agglomerations that formed during calcinations at high temperature. Actual chemical compositions of the BSCF powders were determined by inductive coupled plasma-mass spectrometer (ICP-MS, Perkin-Elmer ELAN6100, USA) and atomic absorption spectrometer (AAS, Perkin-Elmer AAnalyst 600, USA) and are listed in Table 1. Although the actual Ba/Sr and Co/Fe ratio was almost same to those of the target chemical formula, A site (barium and strontium) of the obtained BSCF powders were slightly deficient relative to the B site (cobalt and iron) compared with a targeting chemical formula.

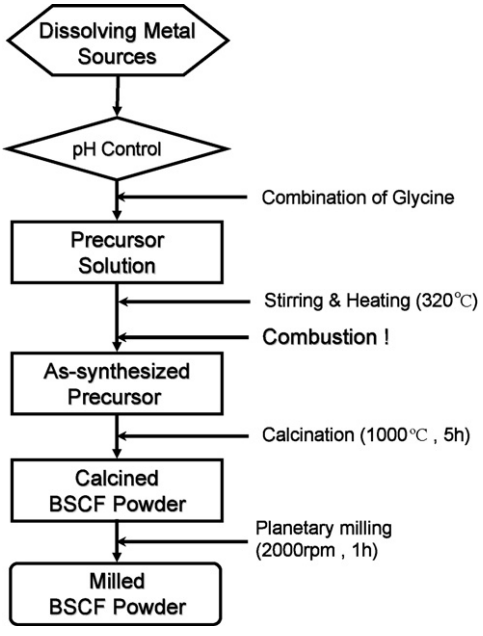

Fig. 1. The procedure for fabrication of $(Ba_{0.5}Sr_{0.5})_{0.99}Co_xFe_{1-x}O_{3-\delta}$ ($x = 0.2$, 0.4, 0.6, and 0.8) by a glycine-nitrate process.

Table 1
Target and actual composition of the BSCF powder

Target composition	Actual composition (at%)			
	Ba	Sr	Co	Fe
$Ba_{0.495}Sr_{0.495}Co_{0.2}Fe_{0.8}O_{3-\delta}$	0.43	0.45	0.19	0.81
$Ba_{0.495}Sr_{0.495}Co_{0.4}Fe_{0.6}O_{3-\delta}$	0.44	0.46	0.40	0.60
$Ba_{0.495}Sr_{0.495}Co_{0.6}Fe_{0.4}O_{3-\delta}$	0.44	0.46	0.60	0.40
$Ba_{0.495}Sr_{0.495}Co_{0.8}Fe_{0.2}O_{3-\delta}$	0.45	0.46	0.79	0.21

2.2. Cell fabrication

An electrolyte-supported symmetric BSCF/ScSZ($89ZrO_2$–$10Sc_2O_3$–$1CeO_2$)/BSCF cell with GDC ($90CeO_2$–$10Gd_2O_3$) buffer layers, which were inserted between the BSCF cathode and ScSZ electrolyte, was fabricated. First, commercially available ScSZ powder ($89ZrO_2$–$10Sc_2O_3$–$1Al_2O_3$, Japan Fine Ceramics Co. Ltd., Japan) was pressed into a pellet and sintered at 1400 °C for 3 h under air. A ScSZ disk with a diameter of 12 mm and a thickness of 1 mm was obtained. A GDC buffer layer was formed on the ScSZ electrolyte by a screen printing technique, and subsequently heat-treated at 1200 °C for 2 h under air. The GDC paste was prepared by mixing a commercially available GDC powder ($90CeO_2$–$10Gd_2O_3$, Anan Kasei Co. Ltd., Japan) and an organic vehicle (α-terpinol, *n*-butyl acetate, and ethyl cellulose). A weight ratio of organic vehicle to GDC powder was 0.43. The GDC buffer layer was formed to prevent unfavorable solid-state reactions at the BSCF/ScSZ interface. A BSCF cathode layer was formed on the GDC buffer layer by a screen printing technique, and then heat-treated at 1000 °C for 2 h. The BSCF cathode paste was prepared by mixing 1000 °C-calcined BSCF powder and an organic vehicle (weight ratio of organic vehicle/BSCF powder is 0.43). The area of the BSCF electrode is 0.5 cm^2, and the cathode retained sufficient porosity. A current-collecting platinum layer containing 15 wt% GDC powder was further formed onto each of the electrodes for reproducibility of the experiment.

2.3. Characterization

Phase identification of the synthesized powders, which were calcined at various temperatures, was performed with a powder diffractometer (MAC Science Co. Ltd., Japan) with Ni-filtered Cu Kα radiation. Cross-sections of the symmetrical cells hav-

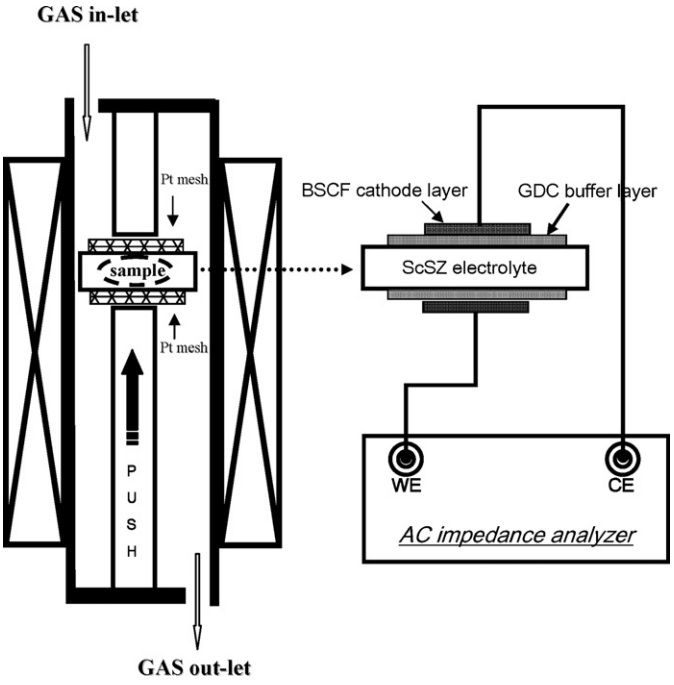

Fig. 2. Schematic diagram of the electrochemical measurement process.

ing a BSCF electrode were observed by field emission scanning electron microscopy (JEOL, JSM-6700F, and TOPCON, SM 300). The thermal expansion coefficients of the BSCF were measured using a dilatometer (LINSEIS, L75/N1). Cylinder type samples with a diameter of 5 mm and a length of 20 mm were used for the thermal expansion coefficient measurement. The electrochemical properties of the BSCF cathodes were measured in a two-electrode symmetric cell configuration under air. AC impedance measurement was performed using a Solartron 2160/1287 electrochemical interface under an open circuit condition from 1 MHz to 0.05 Hz. Fig. 2 shows a schematic diagram illustrating AC impedance measurement.

3. Results and discussion

XRD patterns of the BSCF powders calcined at 1000 °C for 5 h are shown in Fig. 3. Four kinds of BSCF powders were prepared from precursor solutions with different pH values. The BSCF powder prepared from precursor solutions with pH values of 1, 2, and 3 exhibited almost the same characteristic peaks, indicating that BSCF with a single phase perovskite structure could be obtained after calcination at 1000 °C. Use of a highly acidic precursor solution increased the single phase formation temperature.

Glycine ($C_2H_5NO_2$) is composed of an amine group (–NH_2) and a carboxyl group (–COOH). Generally, alkali metals and alkali earth metals are coordinated with a carboxyl group, while transition metals are coordinated with an amine group. When the pH value of the precursor solution is 2.34, the amine groups are 100% ionized. However, the carboxyl groups are 50% ionized while 50% exist in the form of COOH [19]. Accordingly, when the pH value of the precursor solution is less than 1, most carboxyl groups are not ionized and the carboxyl groups become less coordinated with alkali metals and alkali earth metals. It is considered that Ba and Sr cannot complex by the carboxylic acid group of glycine, because under a highly acidic condition the caboxylic group mainly combines with H^+ instead of alkali and alkaline earth metal cations. The loss of binding with glycine results in selective precipitation of the Ba and Sr when the precursor solution is concentrated by boiling. In the case of using a precursor solution with pH 2–3, a single perovskite phase was obtained at 1000 °C.

Based on the results described above, we selected a pH value of 2 for the precursor solution for BSCF synthesis. Fig. 3(b) shows XRD patterns of the BSCF powder, which was prepared from the precursor solution with a pH value of 2 and calcined at various temperatures. As is evident in Fig. 3(b), temperature higher than 900 °C is needed to obtain a single phase perovskite structure. The crystalinity of the BSCF powder was increased as the calcination temperature increased. The effect of composition variation on the phase evolution of the BSCF powder is shown in Fig. 3(c). The XRD patterns of the BSCF powders with different Co content, which were calcined at 1000 °C for 5 h, are quite similar. This indicates that a molar ratio change of Co and Fe does not influence the crystallization behavior of BSCF.

As is also evident from Fig. 3(c), there is, if little, no peak shift with respect to the x value in $(Ba,Sr)Co_xFe_{1-x}O_{3-\delta}$. XRD peaks of BSCF might be shifted to a higher degree as a function of the x value since the ionic radius of Co^{4+} (0.067 nm for six coordination number) is smaller than that of Fe^{4+} (0.0725 nm for six coordination number) [12]. On the other hand, since Co^{4+} and Fe^{4+} in the B-site of the BSCF crystal structure would be reduced to Co^{3+} and Fe^{3+} and the ionic radii of Co^{3+} (0.075 nm) and Fe^{3+} (0.0785 nm) are larger than those of Co^{4+} and Fe^{4+}, the lattice would expand with increasing x value in BSCF. In other words, the lattice shrinkage due to Co substitution might be compensated by lattice expansion due to the reduction of the Co and Fe ions.

Fig. 4 shows the linear thermal expansion versus temperature curves of sintered BSCF samples with different x values. All the curves show a linear relationship between the temperature and the thermal expansion in a temperature range of room temperature to 400 °C. The inflection point of the thermal expansion curve is observed at around 400 °C, and the slope of $\Delta L/L_o$ (thermal expansion coefficient) is slightly increased. The observed inflection of the curves is thought to be due to a loss of oxygen (i.e., the formation of oxygen vacancies) in the BSCF structure during heat-treatment, and this phenomenon might be associated with the reduction of Co and Fe for compensating the charge neutrality of the crystal by the formation of oxygen vacancies.

It is well known that increasing Co content causes an increase in the thermal expansion coefficient of cathode materials containing cobalt in the B site of a perovskite crystal structure [22,23]. A similar trend was also observed in this study. Thermal expansion coefficients of BSCF are 24.0×10^{-6}, 25.8×10^{-6}, 28.6×10^{-6}, and $31.3 \times 10^{-6}\,K^{-1}$ for BSCF ($x = 0.2$), BSCF ($x = 0.4$), BSCF ($x = 0.6$), and BSCF ($x = 0.8$), respectively (in a temperature range of 400–1000 °C). The thermal expansion coefficient of BSCF ($x = 0.8$) ($31.3 \times 10^{-6}\,K^{-1}$) was slightly higher than that of BSCF having the same composition reported

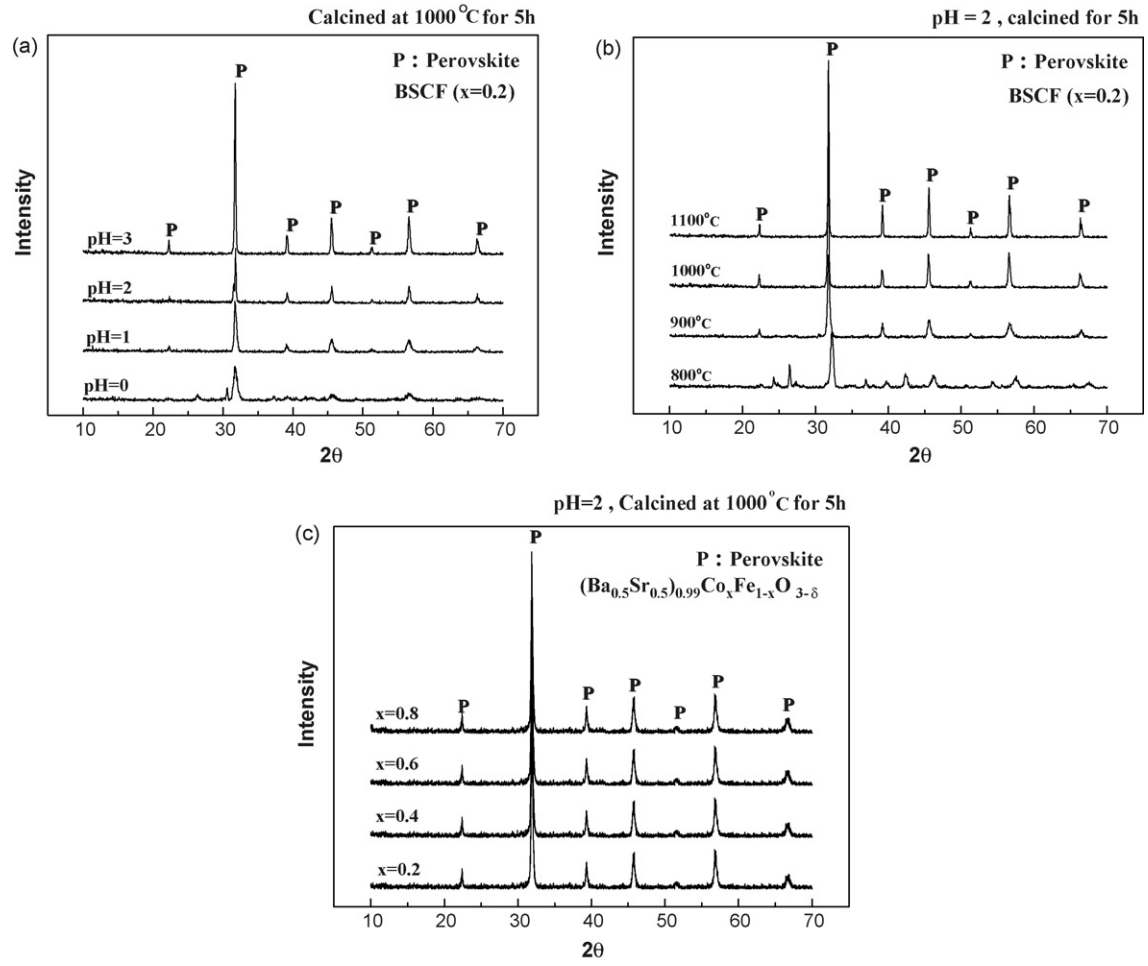

Fig. 3. (a) XRD patterns of BSCF powders synthesized from precursor solutions with various pH values, (b) XRD patterns of BSCF powders calcined at various temperatures (the pH value of the precursor solution is 2), and (c) XRD patterns of BSCF ($x = 0.2$, 0.4, 0.6, and 0.8) powders calcined at 1000 °C for 5 h (the pH value of the precursor solution is 2).

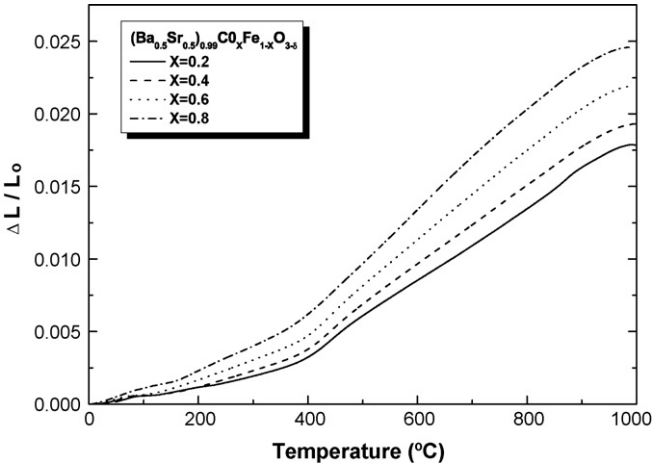

Fig. 4. Thermal expansion vs. temperature curves of $(Ba_{0.5}Sr_{0.5})_{0.99}Co_x Fe_{1-x}O_{3-\delta}$ ($x = 0.2$, 0.4, 0.6, and 0.8).

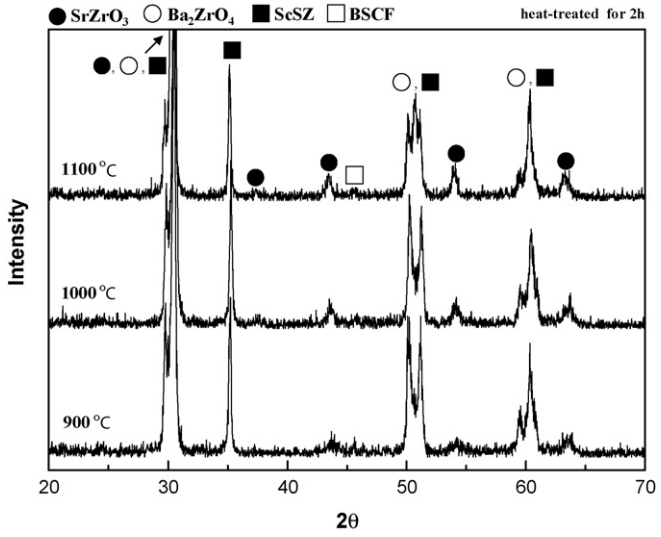

Fig. 5. X-ray diffraction patterns of BSCF ($x = 0.2$)-ScSZ powder mixtures heat-treated at various temperatures. $SrZrO_3$ (JCPDS 76-0167), Ba_2ZrO_4 (JCPDS 77-0944).

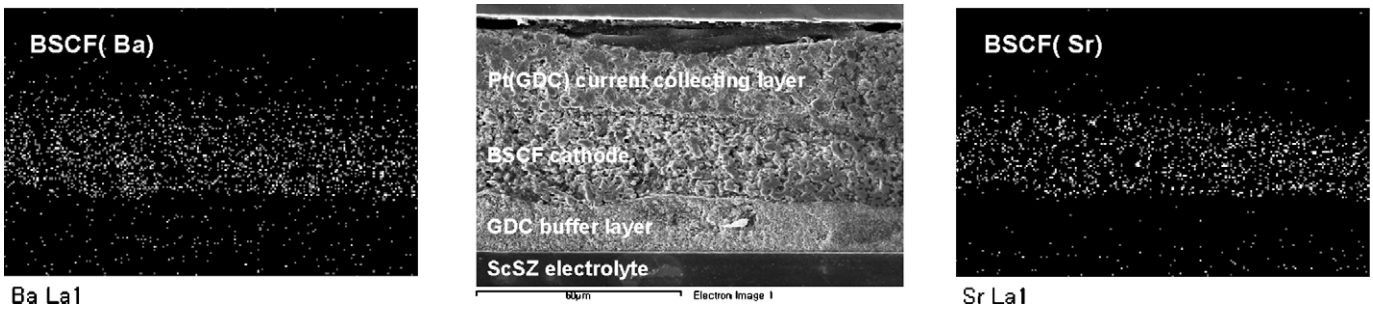

Fig. 6. EDS elemental dot mapping analysis of the cross-section of the BSCF ($x = 0.2$) cathode.

by Wei et al. ($24.26 \times 10^{-6}\,K^{-1}$, 500–1000 °C) [12]. A barium and strontium deficiency in the perovskite crystal structure, density of the sample, and partly measurement system might be responsible for the observed discrepancy.

The interface stability between the BSCF cathode and ScSZ electrolyte is an important issue to be considered. In our previous study, we confirmed that $La_{0.8}Sr_{0.2}Co_{0.2}Fe_{0.8}O_3$ (LSCF) reacts with ScSZ to form strontium zirconate ($SrZrO_3$) and lanthanum zirconate ($La_2Zr_2O_7$) phases [15,16]. In this study, the compatibility between BSCF and ScSZ was investigated by heating a BSCF and ScSZ powder mixture. As is apparent in Fig. 5, BSCF reacted with ScSZ to produce unwanted interfacial phases, even at 900 °C, and their fraction increased with increasing calcination temperature. From the XRD patterns, the interfacial phase was confirmed to be $SrZrO_4$ and Ba_2ZrO_4.

Fig. 6 shows SEM micrographs of the cross-section of the BSCF ($x = 0.2$)/GDC/ScSZ/GDC/BSCF cell sintered at 1000 °C. Energy dispersive X-ray (EDX) elemental dot mapping (Ba and Sr) results are also presented in Fig. 6. There was no evidence of diffusion of Ba and Sr elements in the BSCF cathode in the region

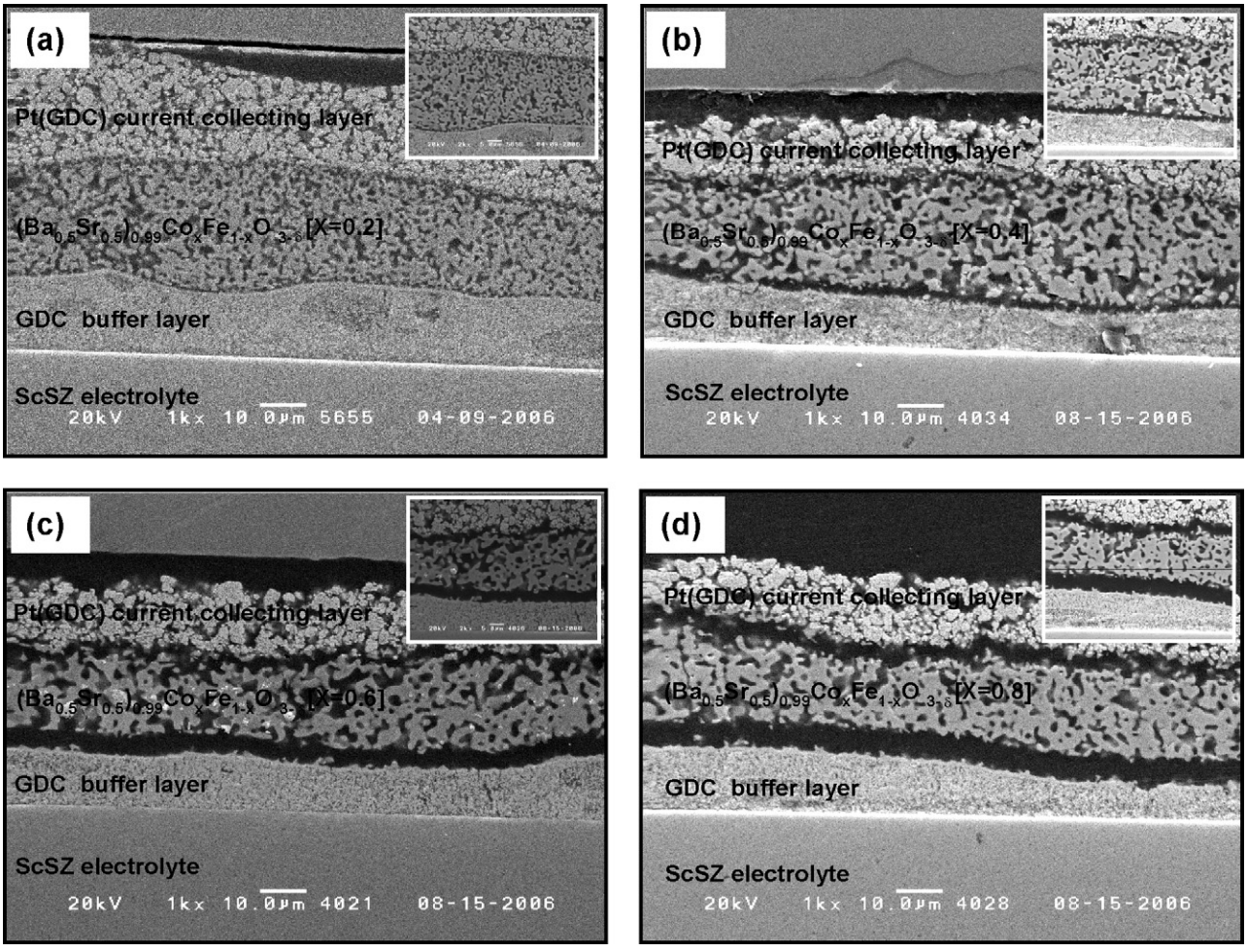

Fig. 7. SEM micrographs showing cross-section of the interface of BSCF ($x = 0.2$)/GDC/ScSZ (a), BSCF ($x = 0.4$)/GDC/ScSZ (b), BSCF ($x = 0.6$)/GDC/ScSZ (c), BSCF ($x = 0.8$)/GDC/ScSZ, and (d) heat-treated at 1000 °C for 2 h.

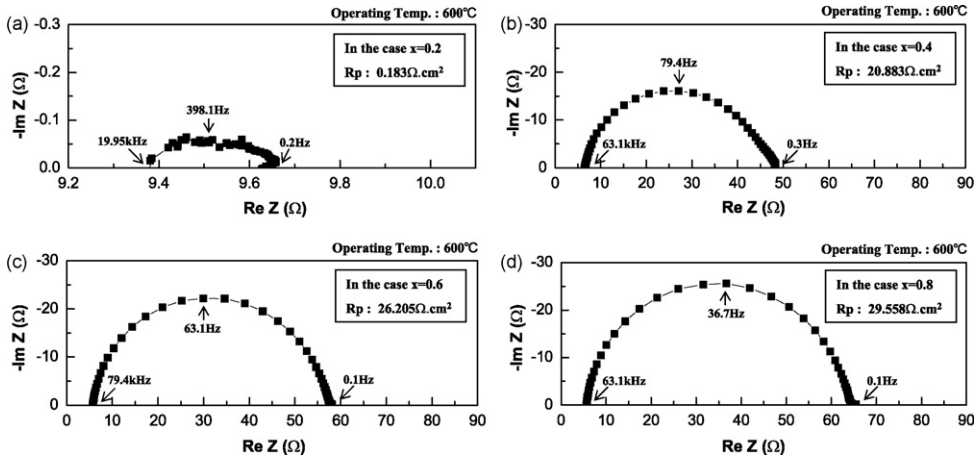

Fig. 8. Impedance spectra of $(Ba_{0.5}Sr_{0.5})_{0.99}Co_xFe_{1-x}O_{3-\delta}$/ScSZ/$(Ba_{0.5}Sr_{0.5})_{0.99}Co_xFe_{1-x}O_{3-\delta}$ symmetrical cells with a GDC buffer layer for $x=0.2$ (a), $x=0.4$ (b), $x=0.6$ (c), and $x=0.8$ (d).

of the GDC buffer layer or at the interface between BSCF and GDC. It can therefore be inferred that the GDC buffer layer effectively blocks the interfacial-reaction between the BSCF cathode and ScSZ electrolyte.

Cross-sections of the BSCF ($x=0.2$, 0.4, 0.6, and 0.8) cathode sintered at 1000 °C for 2 h were observed by SEM. Typical images are shown in Fig. 7. The BSCF cathodes and the platinum electrode were approximately 30 and 20 μm thick, respectively. The BSCF ($x=0.2$) cathode and GDC buffer layer were sufficiently porous and exhibited good interfacial contact with the GDC and ScSZ electrolyte, respectively, with no sign of delamination. As shown in Figs. 7(b–d), a peeling-off phenomenon was observed in BSCF ($x=0.4$), BSCF ($x=0.6$), and BSCF ($x=0.8$), and became more serious as the Co content of BSCF was increased. This phenomenon appears to be due to the high thermal expansion coefficient of BSCF ($x=0.4$, 0.6, and 0.8). In the case of BSCF ($x=0.8$), the thermal expansion coefficient was high ($31.3\times10^{-6}\,K^{-1}$) (400–1000 °C), roughly three times larger than that of ScSZ [24] and GDC [25].

Fig. 8 shows the impedance spectra of the four BSCF cathodes measured at 600 °C under air from 1 MHz to 0.05 Hz. The area of the cathode was 0.5 cm^2 and the area specific resistance (ASR) of BSCF was measured. The ASR values of the BSCF ($x=0.2$), BSCF ($x=0.4$), BSCF ($x=0.6$), and BSCF ($x=0.8$) were estimated to be approximately 0.183, 20.883, 26.205, and 29.558 Ω cm^2, respectively, at an operating temperature of 600 °C. The lower ASR value for BSCF ($x=0.2$) and higher ASR values for BSCF ($x=0.4$–0.8) are consistent with the microstructure at the BSCF/GDC interfaces shown in Fig. 7. The BSCF ($x=0.2$) cathode, which shows good adhesion to the GDC buffer layer, has a much lower ASR value than the other BSCF cathodes, which delaminated from the GDC buffer layer as a result of the large thermal expansion mismatch between BSCF and GDC. Thus, the high ASR value observed in the BSCF ($x=0.4$, 0.6, and 0.8)/GDC/ScSZ cells is considered to be associated with the delamination of the BSCF cathode.

The polarization resistance versus temperature relationship as a function of Co content is exhibited in Fig. 9. From the slope of the curves, the activation energy can be calculated. The activation energy values were 98.95, 132.91, 143.44, and 142.47 kJ mol^{-1} for the BSCF ($x=0.2$), BSCF ($x=0.4$), BSCF ($x=0.6$), and BSCF ($x=0.8$) cathodes, respectively. All electrodes displayed high activation energy except the BSCF ($x=0.2$) cathode. Morphologically unstable cathodes are expected to yield poor electrochemical performance and their activation energies will be very high. On the other hand, the activation energy of the BSCF ($x=0.2$) (Ea = 98.95 kJ mol^{-1}) cathode is much lower than that of other cathode materials. For example, the activation energy for LSCF was estimated to be 135–142 kJ mol^{-1} in our previous report [18]. Thus, BSCF is expected to show much lower polarization resistance than LSCF, especially at lower temperatures.

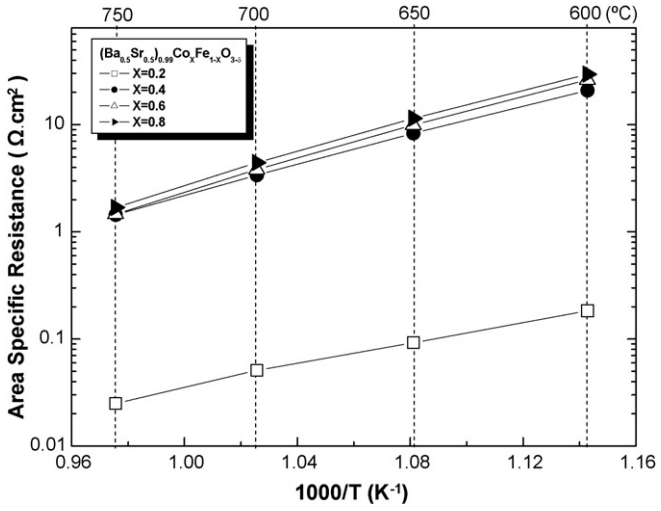

Fig. 9. The area specific resistance (ASR) of BSCF/GDC/ScSZ cells as a function of temperature.

4. Conclusions

BSCF cathode materials were synthesized by a combined glycine nitrate process (GNP). Symmetrical BSCF/GDC/ScSZ/GDC/BSCF cells were fabricated and the electrochem-

ical performance of BSCF was investigated from impedance spectra at extremely low current density. A comparative study was also carried out to investigate the effects of the x value in (Ba,Sr)$Co_xFe_{1-x}O_{3-\delta}$. The following conclusions could be drawn from this study.

(1) Single phase perovskite could be obtained by calcining the gelled BSCF powders at temperatures above 900 °C. The phase evolution behavior of BSCF depended on the pH value of the precursor solution, and not on the composition of the BSCF.
(2) The thermal expansion coefficient was gradually increased with the content of Co.
(3) A GDC buffer layer could effectively control the interfacial-reaction between the BSCF cathode and ScSZ electrolyte. There was no indication of diffusion of strontium or barium in the GDC buffer layer.
(4) Although the thermal expansion coefficient of BSCF ($x = 0.2$) is still larger than that of GDC or ScSZ, the BSCF ($x = 0.2$) cathode adhered well to the GDC buffer layer after heat-treatment at 1000 °C for 2 h. However, we failed to fabricate cells having good contact between other BSCF ($x = 0.4$, 0.6, and 0.8) cathodes and the GDC.
(5) The area specific polarization resistance of the BSCF ($x = 0.2$) cathode was 0.183 $\Omega\,cm^2$ at 600 °C and the activation energy was estimated to be approximately 98.95 kJ mol^{-1}.

Acknowledgement

This work was supported by INHA UNIVERSITY Research Grant.

References

[1] R. O'Hayre, S.W. Cha, W. Colella, F.B. Prinz, Fuel Cell Fundamentals, Wiley, New York, USA, 2006.
[2] G. Hoogers, Fuel Cell Technology, CRC, USA, 2003.
[3] S.C. Singhal, K. Kendall, High Temperature Solid Oxide Fuel Cells: Fundamentals, Design and Applications, Elsevier, Oxford, UK, 2003.
[4] B.C.H. Steele, A. Heinzel, Nature 414 (2001) 345.
[5] I. Yasuda, K. Ogasawara, M. Hishnuma, T. Kawada, M. Dokiya, Solid State Ionics 86–88 (1996) 1197.
[6] G.Ch. Kostogloudis, Ch. Ftikos, Solid State Ionics 126 (1999) 143.
[7] S.P. Jiang, Solid State Ionics 146 (2002) 1.
[8] L.W. Tai, M.M. Nasallah, H.U. Anderson, D.M. Sparlin, S.R. Sehlin, Solid State Ionics 76 (1995) 259.
[9] L.W. Tai, M.M. Nasallah, H.U. Anderson, D.M. Sparlin, S.R. Sehlin, Solid State Ionics 76 (1995) 273.
[10] B.C.H. Steele, J.M. Bae, Solid State Ionics 106 (1998) 255.
[11] Z. Shao, S.M. Halle, Nature 431 (2004) 170.
[12] B. Wei, Z. Lu, X. Huang, J. Miao, X. Sha, X. Xin, W. Su, J. Eur. Ceram. Soc. 26 (2006) 2827.
[13] J. Pena-Martinez, D. Marrero-Lopez, J.C. Ruiz-Morales, B.E. Buergler, P. Nunez, L.J. Gauckler, J. Power Sources 159 (2006) 914.
[14] Q.L. Liu, K.A. Khor, S.H. Chan, J. Power Sources 161 (2006) 123.
[15] H.J. Hwang, C.M. Whang, J.W. Moon, M. Awano, J. Ceram. Soc. Jpn. 112 (2004) S1046.
[16] H.J. Hwang, J.W. Moon, Y.H. Lim, S.H. Lee, E.A. Lee, J. Kor. Ceram. Soc. 42 (2005) 787.
[17] A. Mai, V.A.C. Haanappel, F. Tietz, D. StÖver, Solid State Ionics 177 (2006) 2103.
[18] J.W. Moon, Y.H. Lim, Y.K. Oh, M.J. Lee, B.H. Choi, H.J. Hwang, J. Kor. Ceram. Soc. 42 (2005) 800.
[19] McMurry, Organic Chemistry, Brooks/Cole, USA, 2000.
[20] Y. Ji, J. Liu, T. He, L. Cong, J. Wang, W. Su, J. Alloys Compd. 353 (2003) 257.
[21] H.S. Potdar, S.B. Deshpande, Y.B. Khollam, A.S. Deshpande, S.K. Date, Mater. Lett. 57 (2003) 1066.
[22] N.Q. Minh, J. Am. Ceram. Soc. 76 (1993) 563.
[23] L.W. Tai, M.M. Nasrallah, H.U. Anderson, D.M. Sparlin, S.R. Sehlin, Solid State Ionics 76 (1995) 259.
[24] D. Lee, I. Lee, Y. Jeon, R. Song, Solid State Ionics 176 (2005) 1021.
[25] G. Corbel, S. Mestiri, P. Lacorre, Solid State Sci. 7 (2005) 1216.